# Sequential compound exocytosis of large dense-core vesicles in PC12 cells studied with TEPIQ (two-photon extracellular polar-tracer imaging-based quantification) analysis

Takuya Kishimoto[1,2], Ting-Ting Liu[1,4], Hiroyasu Hatakeyama[1], Tomomi Nemoto[1,3], Noriko Takahashi[1,3] and Haruo Kasai[1,2]

[1]*Department of Cell Physiology, National Institute for Physiological Sciences, and Graduate University of Advanced Studies (SOKENDAI), Myodaiji, Okazaki 444-8787, Japan*
[2]*Center for Disease Biology and Integrative Medicine, Faculty of Medicine, University of Tokyo, Bunkyo-ku, Tokyo 113-0033, Japan*
[3]*Precursory Research for Embryonic Science and Technology (PRESTO), Japan Science and Technology Agency, 4-1-8 Honcho, Kawaguchi, Saitama 332-0012, Japan*
[4]*Genome Research Center, National Yang-Ming University, Taipei, Taiwan*

**We investigated exocytosis of PC12 cells using two-photon excitation imaging and extracellular polar tracers (TEP imaging) at the basal region of PC12 cells adjacent to the glass cover slip. TEPIQ (two-photon extracellular polar-tracer imaging-based quantification) analysis revealed that most exocytosis was mediated by large dense-core vesicles (LVs) with a mean diameter of 220 nm, and that exocytosis of LVs occurred slowly with a mean latency of ∼7 s even though exocytosis was induced with large increases in cytosolic $Ca^{2+}$ concentration by uncaging of a caged-$Ca^{2+}$ compound. We also found that 97% of exocytic LVs remained poised at the plasma membrane, 72% maintained their fusion pores in an open conformation for more than 30 s, and 76% triggered sequential compound exocytosis of vesicles that were located deeper in the cytosol. Sequential compound exocytosis by PC12 cells was confirmed by electron microscopic investigation with photoconversion of diaminobenzidine by FM1-43 (a polar membrane tracer). Our data suggest that pre-stimulus docking of LVs to the plasma membrane does not necessarily hasten the fusion reaction, while docking and resulting stability of exocytic LVs facilitates sequential compound exocytosis, and thereby allowing mobilization of deep vesicles.**

(Received 1 July 2005; accepted after revision 1 September 2005; first published online 8 September 2005)
**Corresponding author** H. Kasai: Department of Cell Physiology, National Institute for Physiological Sciences, Myodaiji, Okazaki 444-8787, Japan. Email: hkasai@nips.ac.jp

Exocytic vesicles are docked to the plasma membrane before stimulation in many secretory cells (Steyer *et al.* 1997; Avery *et al.* 2000; Tsuboi *et al.* 2002). This pre-stimulus docking is thought to facilitate fusion and be a preparatory step for exocytosis (Parsons *et al.* 1995; Neher, 1998). However, it has been noticed that when exocytosis is triggered at the resting level of cytosolic $Ca^{2+}$, docked large dense-core vesicles (LVs) in secretory cells undergo considerably slower fusion (Ninomiya *et al.* 1997; Haller *et al.* 1998; Voets, 2000; Ashery *et al.* 2000) than synaptic vesicles in the active zone (Augustine *et al.* 1985; Sabatini & Regehr, 1996; Bollmann *et al.* 2000; Schneggenburger & Neher, 2000). Thus, the role of pre-stimulus docking of vesicles in preparations lacking the active zone is not fully understood.

To obtain new insight into the processes of exocytosis and endocytosis, we developed two-photon excitation imaging of preparations immersed in polar tracers (TEP imaging), where vesicles are labelled after the fusion reaction (Nemoto *et al.* 2001; Takahashi *et al.* 2002; Kasai *et al.* 2005). Such post-fusion labelling is superior to pre-fusion labelling for tracking the fates of vesicles after fusion, especially when the intercellular space is narrow, and the background fluorescence is low (Kasai *et al.* 2005). Post-fusion labelling shows no selection bias, and exocytosis and endocytosis can be studied in a fully quantitative manner similar to membrane capacitance measurements.

In the current study, we applied TEP imaging and TEPIQ analyses (Kasai *et al.* 2005) to the base of the

T. Kishimoto and T.-T. Liu contributed equally to this work.


DOI: 10.1113/jphysiol.2005.094003

rat pheochromocytoma line, PC12. We succeeded in estimating the diameters of exocytic vesicles as 220 nm. These large dense-core vesicles (LVs) underwent slow exocytosis even though large increases in cytosolic $Ca^{2+}$ were applied by photolysis of a caged-$Ca^{2+}$ compound. We found that LVs remained stably attached to the plasma membrane with an open fusion pore and frequently gave rise to sequential compound exocytosis. We confirmed these observations by electron microscopy (EM).

## Methods

### Cell preparations

A subclone of PC12 cells (B4) was grown in a Dulbecco's modified Eagle's medium-based culture medium in the absence of NGF (nerve growth factor) as previously described (Kishimoto *et al.* 2001). PC12 cells were examined in a recording chamber containing 0.1 mm glass coverslips (Matsunami-glass, Osaka, Japan). The bathing solution for the experiments (SolA) consisted of 140 mM NaCl, 5 mM KCl, 2 mM $CaCl_2$, 1 mM $MgCl_2$, 10 mM glucose, and 10 mM Hepes-NaOH (pH 7.4) (320 mosmolar). Imaging experiments were performed at room temperature (24–25°C).

### Two-photon extracellular polar-tracer (TEP) imaging

TEP imaging was performed as described previously (Kasai *et al.* 2005). The PC12 cells were loaded with 30 $\mu$M nitrophenyl-EGTA (NPE)-acetoxymethyl ester (AM) (Molecular Probes) and, in some experiments, with 10 $\mu$M fura-2FF-AM (TEF Laboratories, Austin, TX, USA). Using a glass pipette one or two of the following fluorescent tracers were applied locally: FM1-43 (25 $\mu$M), sulforhodamine B (SRB; 0.5 mM), or 10 kDa fluorescein dextrans (FD; 2 mM) (Molecular Probes). For washout of dyes, the recording chamber was rapidly superfused with solution lacking dye. Photolysis of NPE was induced with a mercury lamp (U-ULS100HG; Olympus) through a 360 nm band pass filter (Kasai *et al.* 2005). The radiation of the mercury lamp was gated with an electric shutter (IX-ESU; Olympus) with a 125 ms opening duration. The fluorescence of SRB was measured at 570–650 nm (red channel), whereas those of FM1-43, fura-2FF and FD were measured at 400–550 nm (blue channel). The laser power at the specimen was typically 10 mW, and the wavelength was 830 or 850 nm for single- or double-staining, respectively. The control voltages of the photomultipliers were set at 550 and 600 V for the red and blue channels, respectively.

The calibration constants for TEPIQ analyses, $F_E$ and $F_M$, were obtained as described previously (Kasai *et al.* 2005) in the experimental conditions for PC12 cells. In the presence of only SRB, $F_E$ was $223\,432 \pm 4888$ AU $\mu m^{-2}$ (mean ± s.d.). In the presence of both SRB and FM1-43, $F_E$ and $F_M$ were $209\,570 \pm 2500$ AU $\mu m^{-2}$ and $3136 \pm 504$ AU $\mu m^{-2}$, respectively. For the estimation of $F_M$, we used $\beta$-cells, since FM1-43 fluorescence intensity of PC12 cells was about three times greater than predicted by their diameters, as in the case of the membrane capacitance measurement, possibly due to the presence of microvilli in the plasma membrane. For reference, the conversion coefficient ($m_C$) (Kasai *et al.* 2005) was $0.297 \pm 0.048$ (5 $\beta$-cells) in the experimental conditions of this study.

### Photoconversion of DAB and EM analysis

To rapidly fix the cells, the recording chamber (0.5 ml) was superfused (0.2 ml $s^{-1}$) with PBS containing 2% glutaraldehyde within ~5 s of NPE photolysis. The preparations were therefore fixed within 10 s after photolysis. Photoconversion of diaminobenzidine (DAB) by FM1-43 was performed as described previously (Henkel *et al.* 1996; Harata *et al.* 2001). In brief, cells were exposed to the fixative for 20 min and then washed first for 1 h with 100 mM glycine in PBS and then for 5 min with 100 mM ammonium chloride. After an additional brief wash with PBS, the cells were incubated for 20 min with PBS containing DAB (1 mg $ml^{-1}$; Wako, Tokyo, Japan) at pH 7.9. Fluorescence excitation (100 W mercury lamp, 475 nm) was then performed for 8–10 min with the cells in the DAB solution. The cells were subsequently washed for between 1 h and overnight with 100 mM sodium cacodylate buffer (pH 7.4), exposed to 2% osmium tetroxide for 3 h, dehydrated in a series of graded ethanol solutions, and embedded in Epon (Epon 812, TAAB, UK). After incubation for 2 days at 60°C, the coverslip was removed from the Epon with hydrogen flouride, and thin sections (50–60 nm) were cut vertically relative to the surface of the coverslip and mounted on copper grids. The grids were incubated with 2% uranyl acetate for 10 min and with lead solution for 5 min and were then observed by EM (2000EX; Jeol, Tokyo, Japan).

## Results

### $Ca^{2+}$-dependent exocytosis at the base of PC12 cells

We triggered exocytosis in PC12 cells by photolysis of the caged-$Ca^{2+}$ compound NPE-AM, which releases NPE inside of the cells following degradation by intracellular esterases. The rapid increase in the intracellular free $Ca^{2+}$ concentration ($[Ca^{2+}]_i$) caused by NPE photolysis was examined using the indicator fura-2FF. In agreement with previous findings (Nemoto *et al.* 2004), the $[Ca^{2+}]_i$ was estimated to 10–25 $\mu$M in magnitude and > 10 s in duration. We performed TEP imaging with sulforhodamine B (SRB), a fluid-phase polar fluorescent

tracer (Nemoto *et al.* 2001; Takahashi *et al.* 2002) that neither stains nor permeates the plasma membrane. We chose to investigate the basal region of PC12 cells adjacent to the glass coverslip (Fig. 1*A*), which was narrow (20–40 nm; see Fig. 7*A*) and gave rise to low levels of background fluorescence and noise.

Photolysis of NPE resulted in the appearance of many discrete fluorescent spots at the base of the cell (Fig. 1*B*). Three types of events were distinguished from the time courses of fluorescence intensity. In 24% of the events (total of 217 events), the fluorescence intensity showed a single stepwise increase (single events; Figs 1*B* and 2*A*, event 1). The occurrence of single events may be underestimated because their signals were small. In 36% of the events, the increases occurred in a stepwise manner more than once (2–5 times; multi-step events; Figs 1*B* and 2*A*, events 2–4). The full-width-at-half-maximal (FWHM) diameters of the single events (mean = 0.31 $\mu$m, $n = 35$) (Fig. 1*C* and *E*) and the multi-step events (data not shown) were close to the spatial resolution (0.32 $\mu$m) of our two-photon microscope (Kasai *et al.* 2005), and they did not represent the actual diameters of exocytic vesicles.

In the remaining 40% of the events, the fluorescence increases that occurred were not always associated with well-resolved steps (massive events; Figs 1*B* and 2*B*, events 5–10). The mean FWHM diameters of the massive events (0.57 $\mu$m, $n = 42$) were only 1.9-fold larger than those of the single events (Fig. 1*D* and *E*), but they were more than 10 times brighter (Figs 1*D* and 2*B*). The massive events could represent either swelling of vesicles or exocytosis of many vesicles whose individual steps were not well resolved with the 0.3- to 1.5-s time resolution of our imaging system. The following TEPIQ analyses indicated that the latter was the case.

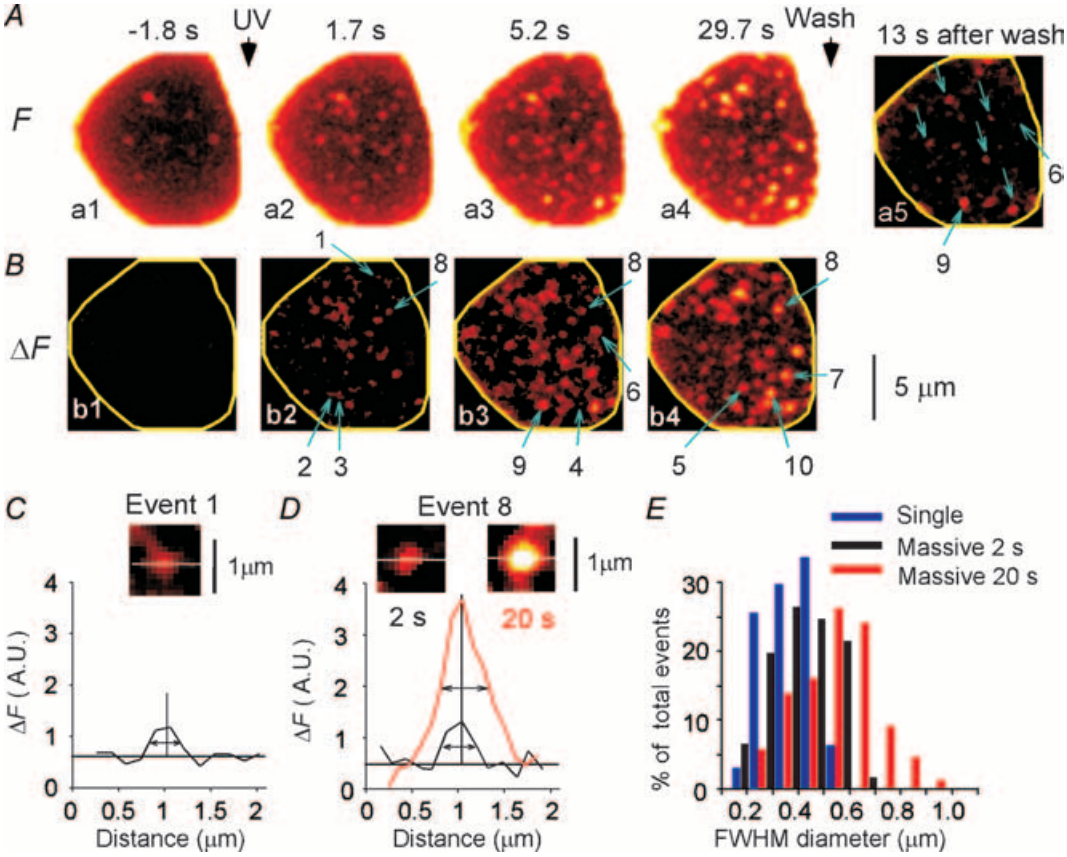


**Figure 1. Two-photon imaging of exocytosis with SRB at the base of a PC12 cell**
*A*, sequential images of SRB fluorescence (*F*) obtained from the base of a cell loaded with NPE-AM and immersed in a solution containing SRB. Photolysis by UV exposure of NPE was induced at a time between frames *a*1 and *a*2. The dye was washed out 50 s after stimulation, and frame *a*5 was obtained 13 s after the wash. Blue arrows in *a*5 indicate spots left after washout. *B*, the difference images ($\Delta F$) shown in frames *b*1 to *b*4 were obtained by subtracting the resting image (frame *a*1) in *A* from frames *a*1 to *a*4, respectively. Fluorescent spots often became brighter over time. Blue arrows in *b*2–*b*4 labelled 1–10 represent the events that are referred in other figures. *C* and *D*, FWHM diameters of single event 1 in *B*, and massive event 8 at 2 s (black) and 20 s after (red) the UV stimulation, respectively. *E*, distributions of FWHM diameters for single (blue), and massive events at 2 s (black) and 20 s (red) after the UV stimulation, respectively.

### TEPIQ analyses of exocytosis in PC12 cells

Using TEPIQ analyses, we estimated the diameters of exocytic vesicles associated with the stepwise events (Fig. 2*A*, arrow heads). TEPIQ analysis of $\Delta V$ predicted the diameters of individual vesicles in the single and multi-step events to be between 0.11 and 0.33 $\mu$m ($0.23 \pm 0.044$ $\mu$m, mean $\pm$ S.D., $n = 95$) (Fig. 3*A*). This value was consistent with the diameter of PC12 cell LVs as determined by EM (see Fig. 7), supporting the idea that the stepwise events reflect the exocytosis of LVs. These findings also suggested that there was no significant binding of SRB to the granule contents.

When exocytosis was visualized in the FM1-43-containing solution (Fig. 3*B*), TEPIQ analysis of $\Delta S$ yielded a vesicle diameter of $0.22 \pm 0.043$ $\mu$m ($n = 36$) for stepwise events (Fig. 3*C*), where $\Delta$S is surface area. The fact that the vesicle diameter determined by TEPIQ analysis of $\Delta S$ was not significantly different from that determined by TEPIQ analysis of $\Delta V$ or from EM studies indicates the absence of staining of the granule matrix by FM1-43 (Angleson *et al.* 1999) in PC-12 cells. TEPIQ analysis of $\Delta V/\Delta S$ yielded a similar estimate of the vesicle diameter ($0.21 \pm 0.059$ $\mu$m, $n = 39$) (Fig. 3*D–F*), indicating that the vesicles were nearly spherical.

We next estimated the average diameters of vesicles involved in the massive events using $\Delta V/\Delta S$-TEPIQ analysis (Fig. 3*G–I*), in order to distinguish whether the massive events were due to many LVs or to swelling of vesicles. This method allows estimation of the diameter even though individual events are not resolved (Kasai *et al.* 2005). The $\Delta V/\Delta S$-TEPIQ diameter should be increased when vesicles swell, since swelling would cause larger influx of SRB in the vesicles relative to that of FM1-43 into the vesicle membranes. We found that the average diameter ($6\Delta V/\Delta S$) was $0.20 \pm 0.049$ $\mu$m ($n = 50$) (Fig. 3*H* and *I*) 10 s after the onset of exocytosis. The diameter was constant in 50% of events (Fig. 3*H*), although a slight increase (6–16%) or decrease (6–17%) was detected in 33% and 17% of events, respectively. This indicates that the massive events were primarily mediated by many vesicles with the diameter of LVs, but not by swelling of vesicles. By dividing the maximal volume of such spots by that of a single LV ($0.005$ $\mu$m$^3$), TEPIQ analyses predicted the number of LVs involved in the multi-step and massive events to be 2–51 ($12 \pm 10$, $n = 89$) (see Fig. 5*B*). When $\Delta V/\Delta S$-TEPIQ analysis was applied to a large region of interest at the base of the cells, it yielded a mean vesicle diameter of $0.19 \pm 0.043$ $\mu$m (8 cells; data not shown), indicating that vesicles at the base of cells were mostly LVs.

### Stability of exocytic LVs in PC12 cells

In striking contrast with insulin granules (Takahashi *et al.* 2002; Kasai *et al.* 2005), most exocytic events in PC12 cells (97%, $n = 217$) stayed at the site of appearance for more than 30 s after exocytosis in PC12 cells (Figs 1*B* and 2). Thus, full fusion events were rare in LV exocytosis (3% of the total) and thus were suppressed in PC12 cells. Moreover, fusion pores kept open for more than 30 s in 72% of vesicles because SRB fluorescence could be washed out (Figs 1*A*, and 4*A* and *B*). This was not because LV exocytosis was studied at the base of the cells on the glass surface, since we also have observed the same phenomenon

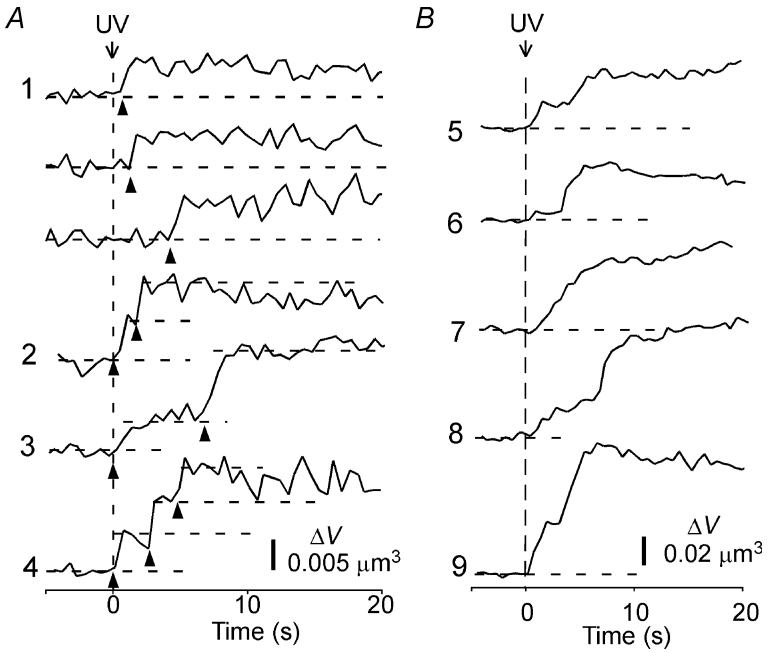


**Figure 2. Analysis of single- and multi-step events**
Time courses of the fluorescence intensity of individual spots for single and multi-step events (*A*) and massive events (*B*). Traces labelled 1–9 correspond to events 1–9 in frames *b*2 to *b*4 in Fig. 3*B*. Arrow heads in *A* indicate individual exocytic events.

at the lateral membrane (Fig. 2*A* and *D* of Liu *et al.* 2005). In 28% of the events, however, fluorescence remained after washout of SRB (Figs 1*Aa*5 (arrows) and 4*C*–*F*), indicating closure of fusion pores, which is often referred to as 'kiss-and-run' (Fesce *et al.* 1994) or direct endocytosis (Ceccarelli *et al.* 1973). The closure of the fusion pore was further supported by the fact that the exocytic vesicles that underwent direct endocytosis reduced their fluorescence (10–90%; mean = 23%, $n = 49$) even in the presence of SRB (Fig. 4*C* and *E*). This was probably due to bleaching of SRB in the endocytic vesicles. In fact, there was little reduction in the fluorescence for events where fusion pores were open (Fig. 1*B*). Direct endocytosis appeared to occur more frequently in single events (55%) than in multi-step or massive events (16%).

Thus, in 72% of the events, exocytic vesicles were stably maintained with open fusion pores for more than 30 s. These stable exocytic vesicles may become a target for deep vesicle exocytosis. Indeed, we found that the fluorescence intensity of 76% of the exocytic spots increased with time (Fig. 1*B*, spots 2–10), often in a stepwise manner (Fig. 2*A*, traces 2–4), suggesting the occurrence of sequential compound exocytosis of LVs. Sequential exocytosis was directly visualized in pancreatic acinar and $\beta$-cells (Nemoto *et al.* 2001; Takahashi *et al.* 2004), which have larger vesicles (diameter of 0.4–1 $\mu$m). It was not straightforward for us to use this approach to demonstrate sequential exocytosis in PC12 cells, because the diameters of the LVs were smaller (0.22 $\mu$m) than the spatial resolution of the optical microscope. The following

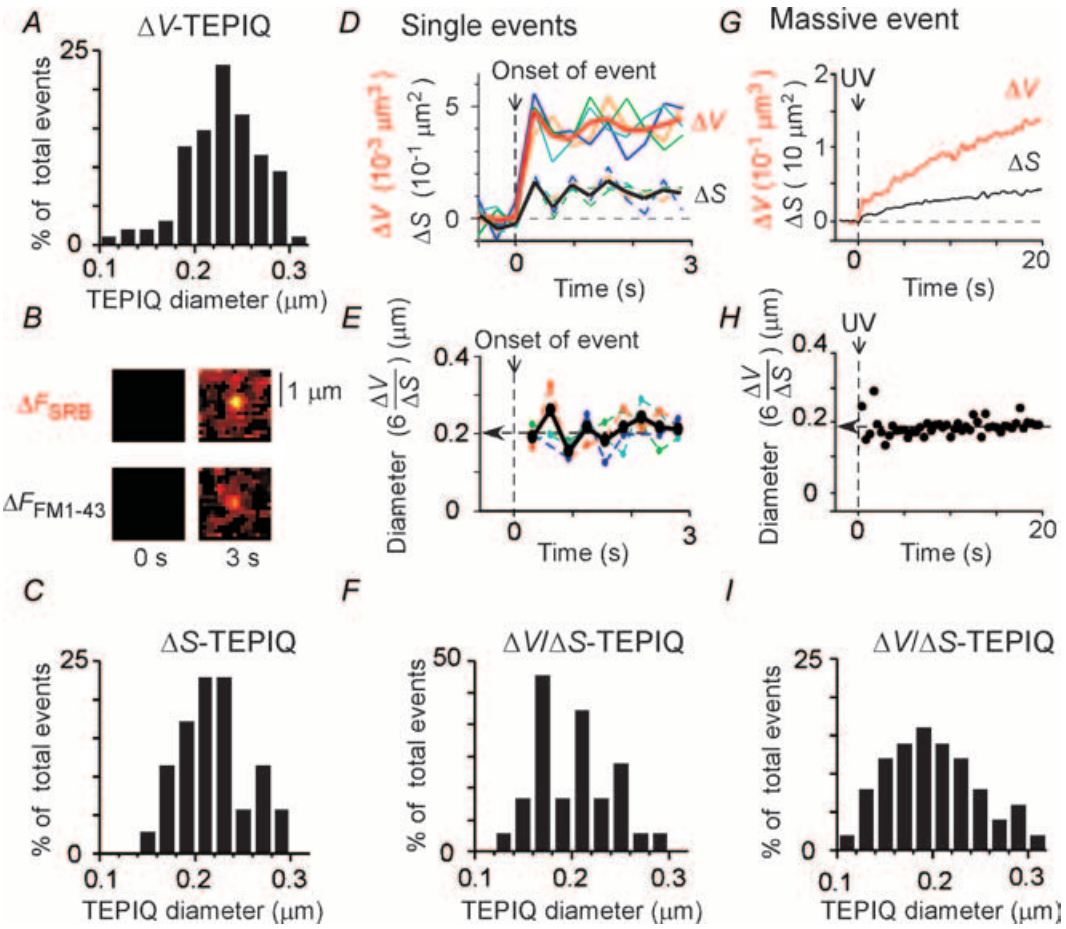


**Figure 3. TEPIQ analyses of LVs in PC12 cells**
*A* and *C*, histograms of vesicle diameter obtained by TEPIQ analyses of $\Delta V$ (*A*) and $\Delta S$ (*C*), respectively, in single events. *B*, multicolour TEP imaging of the exocytosis of a single LV. Shown are the background-subtracted images for SRB ($\Delta F_{SRB}$) and FM1-43 ($\Delta F_{FM1\text{-}43}$) fluorescence before and 3 s after NPE photolysis. *D*, time courses of $\Delta V$ and $\Delta S$ during single exocytic events simultaneously measured with SRB (continuous lines) and FM1-43 (dashed lines). Data for 6 vesicles are aligned at the onset of events. Thick lines show the mean time courses. *E*, time courses of vesicle diameter (6 $\Delta V/\Delta S$) for the data shown in *D*. *F*, a histogram of vesicle diameter obtained by TEPIQ analyses of $\Delta V/\Delta S$ in single events. *G* and *H*, time courses of $\Delta V$ and $\Delta S$ (*G*) and of vesicle diameter (6 $\Delta V/\Delta S$) (*H*) for a massive event. *I*, a histogram of vesicle diameter obtained by TEPIQ analyses of $\Delta V/\Delta S$ in massive events.

observations, however, indicated that the multi-step and massive events mostly reflected sequential compound exocytosis.

### Sequential compound exocytosis of LVs in PC12 cells

The multi-step and massive events were brighter than would be predicted from their FWHM diameters, if they were all LVs that were attached to the plasma membrane at the base of cells. Assuming that an LV has an actual diameter of $d_A$ and a FWHM diameter of $d_F$ (Fig. 5*A*), and that a set of vesicles in a circle at the base of a cell has an apparent FWHM diameters of $d_E$, the number of vesicles in the circle is predicted to be $[(d_E - d_F + d_A)/d_A]^2$ or less (Fig. 5*A*). Therefore, the multi-step or massive events with $d_E$ of 0.53, 0.75 and 0.97 $\mu$m can accommodate at most 4, 9 and 16 LVs at the base of the cell, respectively (the straight line in Fig. 5*B*), given that $d_A$ and $d_F$ are 0.22 $\mu$m and 0.31 $\mu$m, respectively. The actual number of exocytic vesicles estimated from TEPIQ analyses, however, exceeded the theoretical maxima in most (76/89 = 85%) multi-step and massive events (Fig. 5*B*, circles). Even if FWHM diameters were overestimated by 0.1 $\mu$m, 73% of the events would still be outside the region that can be explained by exocytosis at the base of cells (the shaded region in Fig. 5*B*). Many events contained 2–4 times larger numbers of LVs than the theoretical maxima, suggesting that two to four layers of vesicles were involved. These findings indicate that the multi-step and massive events predominantly reflect compound exocytosis of LVs. In fact, EM investigations have detected the prevalence of compound exocytic vesicles (see Fig. 7 and Watanabe *et al.* 1983).

The $\Delta V/\Delta S$-TEPIQ diameters increase by 6–16% in 33% of the massive events, suggesting that the compound vesicles slightly swelled over time. In addition, $\Delta V/\Delta S$-TEPIQ analysis may underestimate the diameter of compound vesicles in the out-of-focal plane (Fig. 8*bE* of Kasai *et al.* 2005) and that, even though $\Delta V/\Delta S$-TEPIQ diameters appeared to be constant, the actual diameter of compound vesicles will increase by 4% when a compound vesicle with a diameter of 0.5 $\mu$m is centred at 0.25 $\mu$m above the focal plane (Fig. 8*E* of Kasai *et al.* 2005). Slight swelling was consistent with electron microscopic images of compound exocytosis in which original individual Ω-profiles were not readily identifiable (see Fig. 7).

TEP imaging revealed that large endocytic vesicles were found after washout of SRB in 16% of the multi-step and massive events (Figs 1*Aa*5 and 4*D*). Such large vesicles were probably generated by compound exocytosis and by '*en block*' endocytosis by closure of a fusion pore. Consistent with this possibility, membrane capacitance measurements in PC12 cells indicate the sudden formation of large endocytic vesicles. Specifically, a stepwise reduction of membrane area reflecting large endocytic vesicles (with a diameter of $>0.5$ $\mu$m if they are spherical) is detected after massive exocytosis of LVs (Kasai *et al.* 1996). Thus, the formation of large compound vesicles is supported by both TEP imaging and membrane capacitance measurements.

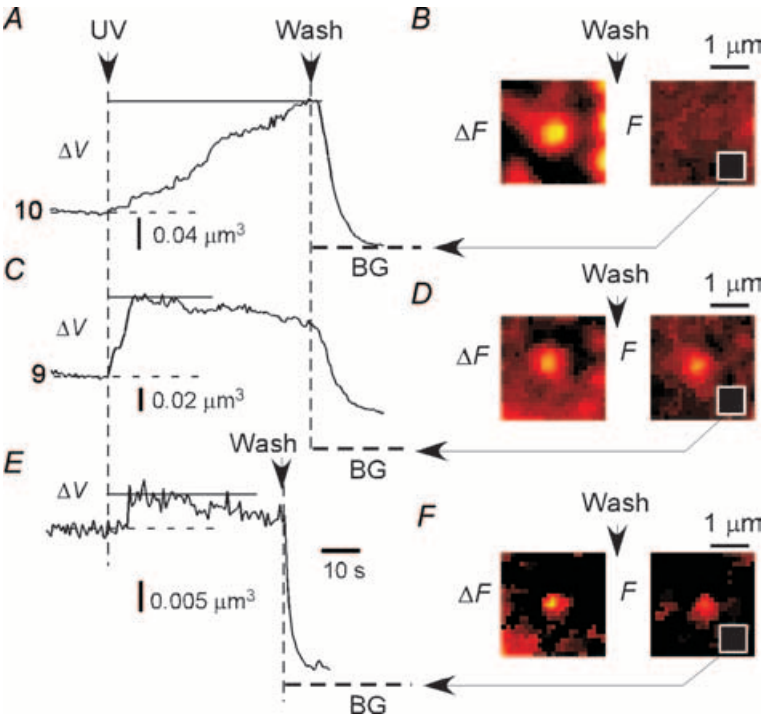


**Figure 4. Behaviours of fusion pores of LVs in PC12 cells**
*A*, *C* and *E*, time courses of fluorescence intensity of massive (*A* and *C*) and single (*E*) events before and after washout of SRB. Fluorescence was either eliminated (*A*) or left unwashed (*C* and *E*). These results indicate that the fusion pore was open in *A* but closed in *C* and *E* by the time of washout. Traces 9 and 10 correspond to respective spots in frames *b*3 and *b*4 of Fig. 3*B*, respectively. Dashed lines labelled BG indicate background fluorescence obtained from white squares in *B*, *D* and *F* after washout of SRB. *B*, *D and F*, fluorescence images for the data shown in *A*, *C* and *E*, respectively. Images on the left (Δ*F*) were obtained by subtraction of baseline images before washout of SRB. Images on the right (*F*) show those after the washout.

We suspect that compound exocytosis in PC12 cells is strictly sequential, in that it does not involve vesicle-to-vesicle fusion events preceding plasma membrane fusion events (multigranular compound exocytosis). Indeed, large stepwise increases in fluorescence were infrequent in our images. Also, time-resolved capacitance measurements do not show large capacitance steps during exocytosis in PC12 cells (Kasai *et al.* 1996), even though they do detect large stepwise reductions in capacitance under the same experiments (Kasai *et al.* 1996). We therefore think that multigranular compound exocytosis is rare in PC12 cells, as in $\beta$-cells (Takahashi *et al.* 2004) and mast cells (Alvarez de Toledo & Fernandez, 1990). In contrast, this form of exocytosis is dominant in eosinophils (Scepek & Lindau, 1993; Hafez *et al.* 2003).

### Time course of large dense-core vesicle exocytosis in PC12 cells

Exocytosis of LVs in single events exhibited a mean latency of 6.8 s (Fig. 6*A*), indicating that surface LVs undergo slow exocytosis in PC12 cells. Well-resolved LV exocytosis in multi-step (Fig. 2*A*, arrowheads) and massive events also showed a similar latency of about 7.4 s (Fig. 6*B*). The long latencies were not due to slow staining of LVs with SRB, because exocytic LVs in PC12 cells were similarly stained by 10 kDa FD (molecular diameter of ~6 nm; $n = 5$; Fig. 6*C* and *D*). The fusion pore thus expanded rapidly to 6 nm, which should allow staining of PC12 LVs by SRB within 1 ms.

Given that exocytic events of LVs were stably maintained after fusion, the time constants for exocytosis of LVs could be obtained from the increase in fluorescence. For the massive events, this value was $7.2 \pm 4.6$ s ($n = 13$). The mean time constant of all LV exocytosis based on the time course of total fluorescence increases was 6.7 s (range, 3–15 s; S.D. = 5.6 s, $n = 8$) at the cell base (data not shown), and 5.7 s (range, 2–10 s; S.D. = 2.6 s, $n = 8$) in the region facing intercellular space (Fig. 3*A* and 5*B* of Liu *et al.* 2005). Thus, all approaches estimated the overall time constants for LV exocytosis to be between 6 and 8 s, in agreement with the results of amperometric measurements (Ninomiya *et al.* 1997; Grishanin *et al.* 2004). We speculate that sequential compound exocytosis proceeded in the cytosol no slower than exocytosis of surface LVs, as in pancreatic acinar cells (Nemoto *et al.* 2001, 2004).

### Ultrastructural identification of exocytic and endocytic vesicles

We examined the ultrastructural correlates of exocytosis at the base of the PC12 cells adjacent to the glass coverslip. The PC12 cell preparations were the same as used for TEP imaging. The sizes of LVs (Fig. 7*A*) were distributed between 0.14 and 0.29 $\mu$m ($0.20 \pm 0.04$ $\mu$m, $n = 95$), in agreement with previous observations (Lowe *et al.* 1988; Tooze *et al.* 1991; Kasai *et al.* 1999). To label $Ca^{2+}$-induced exocytic and endocytic vesicles, we immersed the cells in a FM1-43-containing solution during stimulation, fixed within 10 s after stimulation, and photoconverted the DAB using FM1-43 fluorescence as previously described (Henkel *et al.* 1996; Harata *et al.* 2001). Cells exposed to FM1-43 for only 20 s before fixation had only their plasma membrane stained, while cytosolic organelles were not stained (data not shown).

When the cells were stimulated with photolysis of NP-EGTA, many traces of LV exocytosis were apparent at the base of the cell on the glass coverslips (Fig. 7*B*–*E*). Some vesicles still contained dense matrix, probably reflecting single (Fig. 7*B*, SEx) or compound exocytic events of LVs

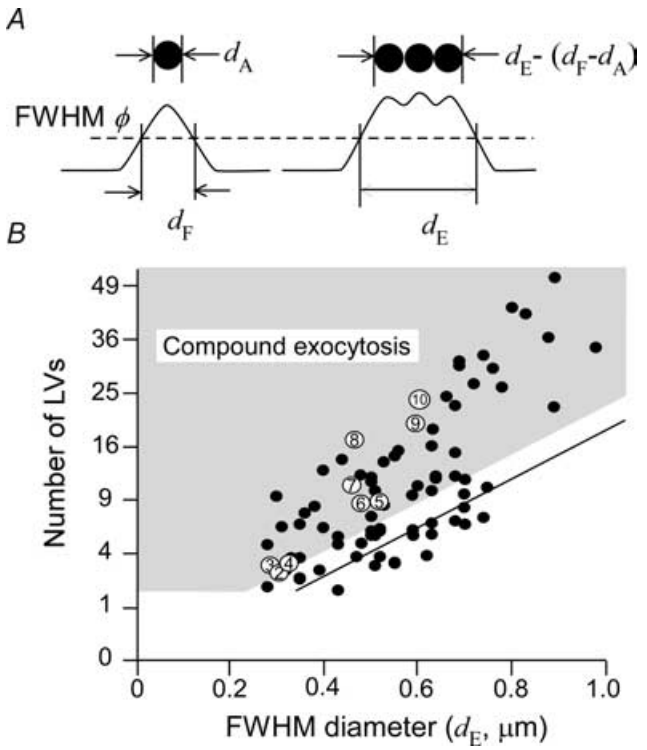


**Figure 5. Relationship between numbers of LVs and FWHM diameters in multi-step and massive exocytic events in PC12 cells**

*A*, relationship between actual diameters of vesicles (upper panels) and their FWHM diameters of fluorescence profiles (lower panels). *B*, the number of LVs involved in each exocytic event plotted against its FWHM diameter, which was estimated by dividing the volume of massive events by that of single events (0.005 $\mu m^3$). The straight line denotes the maximal number of LVs that can be explained by surface vesicles $[(d_E - d_F + d_A)/d_A]^2$. The shaded area represents the events that cannot be accounted for by surface exocytosis at the plasma membrane, taking into account an error of 0.1 $\mu$m in the estimates of FWHM diameters. Open circles with a number denote data obtained from the events shown in Fig. 1*B*.

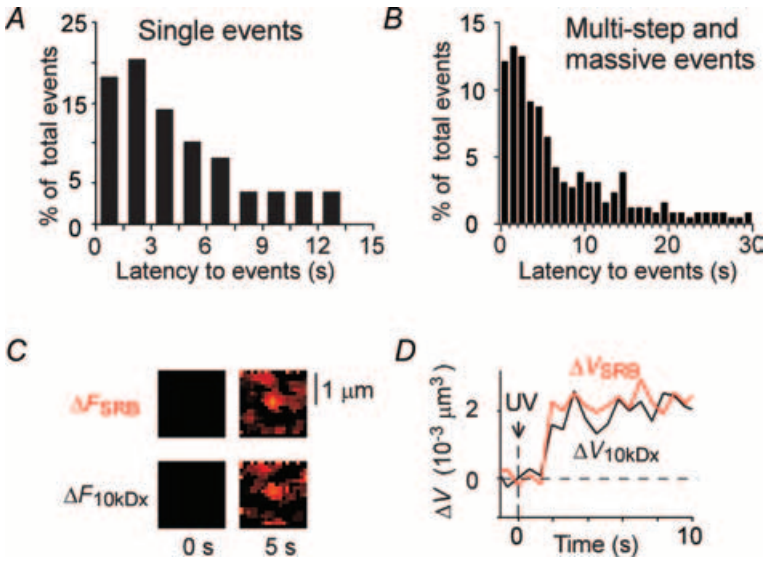


**Figure 6. Time courses of LV exocytosis in PC12 cells**
*A* and *B*, latency histograms for exocytosis of well-resolved individual LV exocytosis for single (*A*) and multi-step and massive events (*B*). *C*, single exocytic events stained by both SRB and 10 kDa FD. The background-subtracted images for SRB ($\Delta F_{SRB}$) and 10 kDa FD ($\Delta F_{10kDax}$) fluorescence before and 5 s after NPE photolysis are shown. *D*, time course of $\Delta V$ estimated by TEPIQ analysis with SRB ($\Delta V_{SRB}$) and 10 kDa FD ($\Delta V_{10kDax}$).

(Fig. 7*B*–*D*, CEx), which were not found in unstimulated control cells (data not shown). These exocytic structures had an opening to the extracellular space, and were found with the spatial frequency of 0.3 $\mu m^{-1}$ at the base of cells (the total length of 78 $\mu$m). In addition to exocytic LVs, we found strongly DAB-positive round vesicles (En in Fig. 7*D* and *E*) with diameters similar to those of LVs ($0.20 \pm 0.035$ $\mu$m, $n = 65$), which were just attached to the plasma membrane without opening to the extracellular space. The fusion pore of these vesicles must be closed,

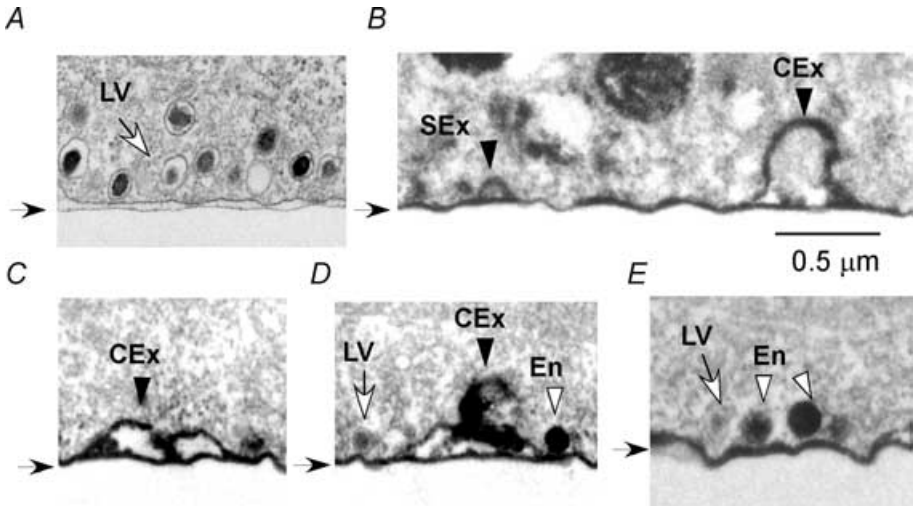


**Figure 7. Ultrastructural identification of exocytic and endocytic vesicles in PC12 cells**
Images were obtained at the base of the cells perpendicular to glass coverslips (black arrows). The surface of the glass appeared irregular due to deformation by tissue processing. *A*, a control cell without stimulation and photoconversion. *B*–*E*, cells immersed in FM1-43 for 20 s and stimulated by photolysis of NPE 10 s after the initial exposure to the tracer and fixed 10 s after photolysis. Photoconversion of DAB was induced by FM1-43 molecules remaining after tracer washout. LV and SEx indicate a single LV before and after exocytosis, respectively. CEx represents compound exocytosis by LVs. En denotes direct endocytic vesicles. The external scale bar (0.5 $\mu$m) in *B* applies to all panels.

as FM1-43 was trapped in the vesicles. These structures reflected direct or 'kiss-and-run' endocytosis of LVs, as predicted from TEP images (Fig. 4*E* and *F*), and were found with a spatial frequency of 0.24 $\mu m^{-1}$. The fact that the endocytic LVs were mostly found attached to the plasma membrane confirmed the persistence of docking after direct endocytosis (Fig. 1*B*). A clustering of LV exocytosis as depicted in Fig. 5*A* (right) has not been detected, supporting the idea that the majority of the massive events reflect compound exocytosis.

The compound exocytosis did not proceed at depths more than 0.8 $\mu$m into the cytosol, and such compound vesicles could not be readily discerned without functional labelling, which labelled excess membranes (Fig. 7*B–D*). The prevalence and diameters (0.4–0.6 $\mu$m) of the compound exocytosis in EM images were consistent with those found in TEP imaging (Figs 1 and 5*B*). Although the compound vesicles were not round, original individual Ω-shapes were not detected in such compound exocytic structures, possibly due to mild swelling of the vesicles or deformation by chemical fixation and photoconversion. Similar ultrastructural features of compound exocytosis were reported in PC12 cells treated with latrotoxin (Watanabe *et al.* 1983). Compound vesicles were always connected with the plasma membrane as indicated by staining of membranes with FM1-43, which supports the absence of multigranular compound exocytosis of LVs in PC12 cells.

## Discussion

We have applied TEPIQ analyses to LV exocytosis of PC12 cells. The diameters of LVs of ∼0.22 $\mu$m calculated with TEPIQ were consistent with the EM studies. Furthermore, we found that many LVs in PC12 cells remained attached to the plasma membrane after fusion, kept their fusion pores open, and gave rise to sequential compound exocytosis (Fig. 8).

### Stable attachment of exocytic LVs in PC12 cells

Many studies have shown that LVs dock at the plasma membrane prior to a stimulus in PC12 cells (Martin & Kowalchyk, 1997; Avery *et al.* 2000; Tsuboi *et al.* 2002). Our data further indicate that LVs stay at the site of exocytosis long after fusion and maintain intact vesicle cavities (Fig. 8). The fact that direct endocytic vesicles also remain attached to the site of exocytosis further supports the existence of mechanisms that keep LVs attached to the plasma membrane even after closure of the fusion pores. Persistent attachment of vesicles was also suggested in pre-fusion labelling studies of exocytosis (Taraska *et al.* 2003; Perrais *et al.* 2004; Tsuboi *et al.* 2004), wherein GFP-labelled proteins stayed at the docking site long after fusion events. Quick-freeze deep-etch EM analysis of chromaffin (Nakata *et al.* 1990) and pituitary cells (Senda *et al.* 1994) has revealed fine strands connecting LVs to the plasma membrane that are sustained after the fusion reaction, and that may reflect annexins (Nakata *et al.* 1990). These data suggest that the pre-stimulus docking reaction can persist even after the fusion reaction (Fig. 8).

Although LVs are tightly docked to the plasma membrane, they undergo relatively slow exocytosis in PC12 cells with a time constant of ∼7 s, suggesting that pre-stimulus docking does not necessarily hasten the fusion reaction. Similarly, the time constant of fusion is about 0.2–1 s even in chromaffin cells wherein exocytosis was induced at the resting $[Ca^{2+}]_i$ level, and was not primed by submicromolar increases in $[Ca^{2+}]_i$ for more than 3 min (Ninomiya *et al.* 1997; Haller *et al.* 1998; Voets *et al.* 1999; Ashery *et al.* 2000). In contrast, the time constant of fusion for synaptic vesicles in the active zone is a fraction of a millisecond even without such $Ca^{2+}$ priming (Llinas *et al.* 1981; Sabatini & Regehr, 1996; Bollmann *et al.* 2000; Schneggenburger & Neher, 2000). Thus, active zone structures and proteins must be utilized for submillisecond fusion reaction of docked vesicles.

### Sequential exocytosis of LVs

Although we found that pre-stimulus docking does not necessarily hasten the fusion reaction, such docking has been reported in many secretory cells (Steyer *et al.* 1997; Martin & Kowalchyk, 1997; Ohara-Imaizumi *et al.* 2004). Thus, it is worth considering the physiological role of pre-stimulus docking. One possibility is that docking persists after fusion reaction, and preserves the Ω-shaped profiles of fused vesicles at the site of exocytosis, thereby facilitating sequential compound exocytosis (Fig. 8). In fact, using TEP imaging in PC12 cells, we have, for the first time, found strong evidence for sequential exocytosis. Importantly, sequential compound exocytosis can easily escape detection by other approaches such as pre-fusion labelling studies, amperometry and membrane capacitance measurements. In contrast to LVs, most

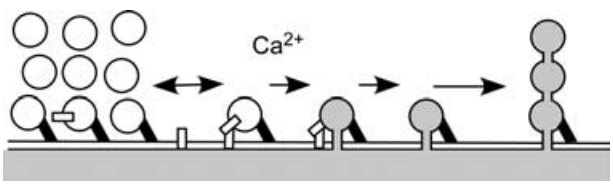


**Figure 8. Pre-stimulus docking and sequential exocytosis**
Vesicles are clustered at the plasma membrane, and remained docked after fusion reaction, keeping their fusion pores open. Such primary exocytic vesicles become targets for subsequent exocytosis of LVs deep in the cytosol. Black bars denote 'intervening strands' connecting between docked vesicles and the plasma membrane. Open bars denote putative proteins involved in membrane fusions.

small vesicles of PC12 cells did not show pre-stimulus docking (Liu *et al.* 2005), readily detached from the plasma membrane after exocytosis, and show no sequential exocytosis (Fig. 9 of Liu *et al.* 2005).

Sequential compound exocytosis is the most efficient mechanism for the mobilization of vesicles deep in the cytosol (Nemoto *et al.* 2001; Takahashi *et al.* 2004), and it is found in many other secretory cells, including exocrine pancreas cells (Ichikawa, 1965; Nemoto *et al.* 2001, 2004; Thorn *et al.* 2004; Pickett *et al.* 2005), $\beta$-cells (Orci *et al.* 1973; Takahashi *et al.* 2004), nasal gland cells (Oshima *et al.* 2005), mast cells (Anderson *et al.* 1973; Alvarez de Toledo & Fernandez, 1990; Guo *et al.* 1998), and pituitary lactotrophs (Angleson *et al.* 1999). In all of these examples, primary vesicles were attached to the site of exocytosis to support secondary exocytosis. Thus, we propose that pre-stimulus docking of vesicles promotes mobilization of deep vesicles via sequential compound exocytosis. In contrast to PC12 cells, sequential exocytosis is relatively infrequent in $\beta$-cells (Takahashi *et al.* 2004), partly because $\Omega$-profiles of insulin granules in $\beta$-cells are unstable and ready to collapse into the plasma membrane (Takahashi *et al.* 2002). The suppression of sequential exocytosis may be relevant to the regulation of insulin exocytosis, which is known to depend critically on cellular energy states (Takahashi *et al.* 2004).

Two-photon excitation imaging has been essential to reveal new features of exocytosis even at the base of PC12 cells, because two-photon excitation enables simultaneous multicolour imaging (Schapper *et al.* 2003), and greatly mitigates heat generation by extracellular tracers (Kasai *et al.* 2005). Since an evanescent wave microscope can only visualize a thin surface layer, it can neither investigate sequential exocytosis, nor estimate diameters of vesicles. TEP imaging can be further utilized to dissect intermediate steps of exocytosis.

## References


Alvarez de Toledo G & Fernandez JM (1990). Compound versus multigranular exocytosis in peritoneal mast cells. *J General Physiol* **95**, 397–409.

Anderson P, Slorach SA & Uvnas B (1973). Sequential exocytosis of storage granules during antigen-induced histamine release from sensitized rat mast cells in vitro. An electron microscopic study. *Acta Physiol Scand* **88**, 359–372.

Angleson JK, Cochilla AJ, Kilic G, Nussinovitch I & Betz WJ (1999). Regulation of dense core release from neuroendocrine cells revealed by imaging single exocytic events. *Nat Neurosci* **2**, 440–446.

Ashery U, Varoqueaux F, Voets T, Betz A, Thakur P, Koch H, Neher E, Brose N & Rettig J (2000). Munc13-1 acts as a priming factor for large dense-core vesicles in bovine chromaffin cells. *EMBO J* **19**, 3586–3596.

Augustine GJ, Charlton MP & Smith SJ (1985). Calcium entry and transmitter release at voltage-clamped nerve terminals of squid. *J Physiol* **367**, 163–181.

Avery J, Ellis DJ, Lang T, Holroyd P, Riedel D, Henderson RM, Edwardson JM & Jahn R (2000). A cell-free system for regulated exocytosis in PC12 cells. *J Cell Biol* **148**, 317–324.

Bollmann JH, Sakmann B & Borst JG (2000). Calcium sensitivity of glutamate release in a calyx-type terminal. *Science* **289**, 953–957.

Ceccarelli B, Hurlbut WP & Mauro A (1973). Turnover of transmitter and synaptic vesicles at the frog neuromuscular junction. *J Cell Biol* **57**, 499–524.

Fesce R, Grohovaz F, Valtorta F & Meldolesi J (1994). Neurotransmitter release: fusion or 'kiss-and-run'? *Trends Cell Biol* **4**, 1–4.

Grishanin RN, Kowalchyk JA, Klenchin VA, Ann K, Earles CA, Chapman ER, Gerona RR & Martin TF (2004). CAPS acts at a prefusion step in dense-core vesicle exocytosis as a PIP2 binding protein. *Neuron* **43**, 551–562.

Guo Z, Turner C & Castle D (1998). Relocation of the t-SNARE SNAP-23 from lamellipodia-like cell surface projections regulates compound exocytosis in mast cells. *Cell* **94**, 537–548.

Hafez I, Stolpe A & Lindau M (2003). Compound exocytosis and cumulative fusion in eosinophils. *J Biol Chem* **278**, 44921–44928.

Haller M, Heinemann C, Chow RH, Heidelberger R & Neher E (1998). Comparison of secretory responses as measured by membrane capacitance and by amperometry. *Biophys J* **74**, 2100–2113.

Harata N, Ryan TA, Smith SJ, Buchanan J & Tsien RW (2001). Visualizing recycling synaptic vesicles in hippocampal neurons by FM 1-43 photoconversion. *Proc Natl Acad Sci U S A* **98**, 12748–12753.

Henkel AW, Lubke J & Betz WJ (1996). FM1-43 dye ultrastructural localization in and release from frog motor nerve terminals. *Proc Natl Acad Sci U S A* **93**, 1918–1923.

Ichikawa A (1965). Fine structural changes in response to hormonal stimulation of the perfused caine pancreas. *J Cell Biol* **24**, 369–385.

Kasai H, Hatakeyama H, Kishimoto T, Liu T-T, Nemoto T & Takahashi N (2005). A new quantitative (two-photon extracellular polar-tracer imaging-based quantification (TEPIQ)) analysis for diameters of exocytic vesicles and its application to pancreatic islets. *J Physiol* **568**, 891–903.

Kasai H, Kishimoto T, Liu T-T, Miyashita Y, Podini P, Grohovaz F & Meldolesi J (1999). Multiple and diverse forms of regulated exocytosis in wild-type and defective PC12 cells. *Proc Natl Acad Sci U S A* **96**, 945–949.

Kasai H, Takagi H, Ninomiya Y, Kishimoto T, Ito K, Yoshida A, Yoshioka T & Miyashita Y (1996). Two components of exocytosis and endocytosis in PC12 cells studied using caged-$Ca^{2+}$ compounds. *J Physiol* **494**, 53–65.

Kishimoto T, Liu T-T, Ninomiya Y, Takagi H, Yoshioka T, Ellis-Davies GC, Miyashita Y & Kasai H (2001). Ion selectivities of the $Ca^{2+}$ sensors for exocytosis in rat phaeochromocytoma cells. *J Physiol* **533**, 627–637.

Liu T-T, Kishimoto T, Hatakeyama H, Nemoto T, Takahashi N & Kasai H (2005). Exocytosis and endocytosis of small vesicle in PC12 cells studied with TEPIQ (two-photon extracellular polar-tracer imaging-based quantification) analysis. *J Physiol* **568**, 917–929.

Llinas R, Steinberg IZ & Walton K (1981). Relationship between presynaptic calcium current and postsynaptic potential in squid giant synapse. *Biophys J* **33**, 323–351.

Lowe AW, Madeddu L & Kelly RB (1988). Endocrine secretory granules and neuronal synaptic vesicles have three integral membrane proteins in common. *J Cell Biol* **106**, 51–59.

Martin TFJ & Kowalchyk JA (1997). Docked secretory vesicles undergo $Ca^{2+}$-activated exocytosis in a cell-free system. *J Biol Chem* **272**, 14447–14453.

Nakata T, Sobue K & Hirokawa N (1990). Conformational change and localization of calpactin I complex involved in exocytosis as revealed by quick-freeze, deep-etch electron microscopy and immunocytochemistry. *J Cell Biol* **110**, 13–25.

Neher E (1998). Vesicle pools and $Ca^{2+}$ microdomains: new tools for understanding their roles in neurotransmitter release. *Neuron* **20**, 389–399.

Nemoto T, Kimura R, Ito K, Tachikawa A, Miyashita Y, Iino M & Kasai H (2001). Sequential-replenishment mechanism of exocytosis in pancreatic acini. *Nat Cell Biol* **3**, 253–258.

Nemoto T, Kojima T, Oshima A, Bito H & Kasai H (2004). Stabilization of exocytosis by dynamic F-actin coating of zymogen granules in pancreatic acini. *J Biol Chem* **279**, 37544–37550.

Ninomiya Y, Kishimoto T, Yamazawa T, Ikeda H, Miyashita Y & Kasai H (1997). Kinetic diversity in the fusion of exocytotic vesicles. *EMBO J* **16**, 929–934.

Ohara-Imaizumi M, Nishiwaki C, Kikuta T, Nagai S, Nakamichi Y & Nagamatsu S (2004). TIRF imaging of docking and fusion of single insulin granule motion in primary rat pancreatic beta-cells: different behaviour of granule motion between normal and Goto-Kakizaki diabetic rat beta-cells. *Biochem J* **381**, 13–18.

Orci L, Malaisse-Lagae F, Ravazzola M, Amherdt M & Renold AE (1973). Exocytosis-endocytosis coupling in the pancreatic beta cell. *Science* **181**, 561–562.

Oshima A, Kojima T, Dejima K, Hisa I, Kasai H & Nemoto T (2005). Two-photon microscopic analysis of acetylcholine-induced mucus secretion in guinea pig nasal glands. *Cell Calcium* **37**, 349–357.

Parsons TD, Coorssen JR, Horstmann H & Almers W (1995). Docked granules, the exocytotic burst, and the need for ATP hydrolysis in endocrine cells. *Neuron* **15**, 1085–1096.

Perrais D, Kleppe IC, Taraska JW & Almers W (2004). Recapture after exocytosis causes differential retention of protein in granules of bovine chromaffin cells. *J Physiol* **560**, 413–428.

Pickett JA, Thorn P & Edwardson JM (2005). The plasma membrane Q-SNARE syntaxin 2 enters the zymogen granule membrane during exocytosis in the pancreatic acinar cell. *J Biol Chem* **280**, 1506–1511.

Sabatini BL & Regehr WG (1996). Timing of neurotransmission at fast synapses in the mammalian brain. *Nature* **384**, 170–172.

Scepek S & Lindau M (1993). Focal exocytosis by eosinophils – compound exocytosis and cumulative fusion. *EMBO J* **12**, 1811–1817.

Schapper F, Goncalves JT & Oheim M (2003). Fluorescence imaging with two-photon evanescent wave excitation. *Eur Biophys J* **32**, 635–643.

Schneggenburger R & Neher E (2000). Intracellular calcium dependence of transmitter release rates at a fast central synapse. *Nature* **406**, 889–893.

Senda T, Okabe T, Matsuda M & Fujita H (1994). Quick-freeze, deep-etch visualization of exocytosis in anterior pituitary secretory cells: localization and possible roles of actin and annexin II. *Cell Tissue Res* **277**, 51–60.

Steyer JA, Horstmann H & Almers W (1997). Transport, docking and exocytosis of single secretory granules in live chromaffin cells. *Nature* **388**, 474–478.

Takahashi N, Hatakeyama H, Okado H, Miwa A, Kishimoto T, Kojima T, Abe T & Kasai H (2004). Sequential exocytosis of insulin granules is associated with redistribution of SNAP25. *J Cell Biol* **165**, 255–262.

Takahashi N, Kishimoto T, Nemoto T, Kadowaki T & Kasai H (2002). Fusion pore dynamics and insulin granule exocytosis in the pancreatic islet. *Science* **297**, 1349–1352.

Taraska JW, Perrais D, Ohara-Imaizumi M, Nagamatsu S & Almers W (2003). Secretory granules are recaptured largely intact after stimulated exocytosis in cultured endocrine cells. *Proc Natl Acad Sci U S A* **100**, 2070–2075.

Thorn P, Fogarty KE & Parker I (2004). Zymogen granule exocytosis is characterized by long fusion pore openings and preservation of vesicle lipid identity. *Proc Natl Acad Sci U S A* **101**, 6774–6779.

Tooze SA, Flatmark T, Tooze J & Huttner WB (1991). Characterization of the immature secretory granule, an intermediate in granule biogenesis. *J Cell Biol* **115**, 1491–1503.

Tsuboi T, McMahon HT & Rutter GA (2004). Mechanisms of dense core vesicle recapture following 'kiss and run' ('cavicapture') exocytosis in insulin-secreting cells. *J Biol Chem* **279**, 47115–47124.

Tsuboi T, Terakawa S, Scalettar BA, Fantus C, Roder J & Jeromin A (2002). Sweeping model of dynamin activity. Visualization of coupling between exocytosis and endocytosis under an evanescent wave microscope with green fluorescent proteins. *J Biol Chem* **277**, 15957–15961.

Voets T (2000). Dissection of three $Ca^{2+}$-dependent steps leading to secretion in chromaffin cells from mouse adrenal slices. *Neuron* **28**, 537–545.

Voets T, Neher E & Moser T (1999). Mechanisms underlying phasic and sustained secretion in chromaffin cells from mouse adrenal slices. *Neuron* **23**, 607–615.

Watanabe O, Torda M & Meldolesi J (1983). The effect of $\alpha$-latrotoxin on the neurosecretory PC12 cell line: electron microscopy and cytotocity studies. *Neuroscience* **3**, 1011–1024.

## Acknowledgements

We thank T. Kanaseki for helpful suggestions and T. Kise, T. Suzuki and N. Takahashi for technical assistance. This work was supported by Grants-in-Aid from the Ministry of Education, Culture, Sports, Science, and Technology of Japan and by research grants from the Human Frontier Science Program Organization, NIH and the Takeda Science Foundation.